Macromolecular Bioscience
www.mbs-journal.de

Nitrilotriacetic Acid Functionalized Microgels for Efficient Immobilization of Hyaluronan Synthase

Isabel Katja Sommerfeld, Esther Maria Dälken, Lothar Elling, and Andrij Pich**

Enzymes play a vital role in synthesizing complex biological molecules like hyaluronic acid (HA). Immobilizing enzymes on support materials is essential for their efficient use and reuse in multiple cycles. Microgels, composed of cross–linked, highly swollen polymer networks, are ideal for enzyme uptake owing to their high porosity. This study demonstrates the immobilization of His_6-tagged hyaluronan synthase from *Pasteurella multocida* (*Pm*HAS) onto nitrilotriacetic acid functionalized microgels using different bivalent ions (Ni^{2+}, Co^{2+}, Mn^{2+}, Mg^{2+}, and Fe^{2+}) via metal affinity binding. The results indicate that using Ni^{2+} yields the microgels with the highest enzyme uptake and HA formation. The immobilized *Pm*HAS enables repetitive enzymatic production, producing high molecular weight HAs with decreasing dispersities in each step. Furthermore, the highest reported yield of HA with high molecular weight for immobilized *Pm*HAS is achieved. This system establishes a foundation for continuous HA formation, with future works potentially enhancing *Pm*HAS stability through protein engineering.

1. Introduction

Hyaluronic acid (HA) is a versatile polysaccharide used extensively in medical[1,2] or cosmetic[3] applications, among others. Its biological functions are largely dependent on its molecular weight. Our study aims to synthesize high molecular weight HA, known for its anti-adhesive, immunosuppressive, and anti-inflammatory properties. This HA variant finds application in wound healing, tissue viscoelasticity restoration, and cartilage degeneration repair.[4,5]

HA is typically produced through either extraction from rooster combs or *Streptococcus* bacteria fermentation, resulting in polydisperse products, potentially contaminated with avian proteins or endotoxins.[5–8] Considering the constraints linked to current mass production methods, whether from animal or bacterial sources, an in vitro production system based on hyaluronan synthase (HAS) is a desirable alternative.[5,8] HAS enzymes are classified into Class I and Class II.[8,9] Class I HAS enzymes are integral membrane proteins, rendering their isolation and purification challenging due to their membrane-bound structure. Without close association with the phospholipid layer, their function is impaired, thereby hindering commercial-scale HA production.[8] In contrast, Class II HAS enzymes, typically encoded by the organism *Pasteurella multocida*, are more readily employed in cell-free HA production.[8,10]

The soluble mutant of HAS from *Pasteurella multocida* (*Pm*HAS1-703) produces high molecular weight HA with low polydispersity.[5,8] However, since the yield of HA remains relatively low, the reuse of *Pm*HAS is required. This presents a challenge as the separation of soluble enzymes from reaction mixtures is complex and time-consuming.[11,12] In contrast, immobilized enzymes enable simple product and enzyme recovery and continuous enzymatic production.[12,13] Immobilization of enzymes on a carrier broadens applications by incorporating diverse functional groups, facilitating surface attachment and selective molecule interaction. The carrier also influences the enzyme's kinetic and mechanical properties, making carrier selection crucial for optimizing enzyme performance.[11,14] While inheriting all the advantages of enzyme immobilization, immobilization on nanosized carriers offers additional benefits. Nanocarriers excel with their high surface-to-volume ratio, enabling a high surface-loading capacity and reducing diffusional limitations.[15,16] An additional increase in enzyme loading[17]

I. K. Sommerfeld, E. M. Dälken, A. Pich
Functional and Interactive Polymers
Institute of Technical and Macromolecular Chemistry
RWTH Aachen University
Worringerweg 2, 52074 Aachen, Germany
E-mail: pich@dwi.rwth-aachen.de
I. K. Sommerfeld, E. M. Dälken, A. Pich
DWI – Leibniz-Institute for Interactive Materials e.V.
Forckenbeckstraße 50, 52074 Aachen, Germany
L. Elling
Laboratory for Biomaterials
Institute of Biotechnology and Helmholtz-Institute for Biomedical Engineering
RWTH Aachen University
Pauwelsstraße 20, 52074 Aachen, Germany
E-mail: l.elling@biotec.rwth-aachen.de
A. Pich
Aachen Maastricht Institute for Biobased Materials (AMIBM)
Maastricht University
Brightlands Chemelot Campus
Urmonderbaan 22, RD Geleen 6167, The Netherlands

The ORCID identification number(s) for the author(s) of this article can be found under https://doi.org/10.1002/mabi.202400075

DOI: 10.1002/mabi.202400075

and a decrease in diffusional limitations[16] can be realized through high porosity.

Microgels are soft, cross–linked, highly swollen polymer networks[18] and possess distinct properties that differentiate them from rigid nanocarriers like silica particles, zeolites, magnetic nanoparticles, or rigid polymer particles.[11] Microgels stand out due to their exceptionally high water content and porosity, enabling high enzyme loading efficiency and efficient substrate diffusion compared to other carriers.[11] Employing a core–shell morphology allows specific enzyme localization,[11,19] with the microgel core having higher crosslinking density and the shell creating a fuzzy, porous surface.[20] This design allows enzyme immobilization on the porous microgel shell, enhancing substrate diffusion. Simultaneously, the cross–linked microgel core maintains the microgels' structural integrity and enables simple separation from products through centrifugation. In addition to these unique properties, microgels exhibit high biocompatibility and achieve enzyme activities similar to rigid particles.[11]

Having established the advantages of microgels for enzyme immobilization, enzyme attachment to a microgel carrier can be achieved through covalent attachment, ionic binding, or weak interactions.[14] While each approach offers advantages, they also present disadvantages such as weak binding,[11,14] distortion of kinetics,[21] irreversible binding,[14] and enzyme deactivation.[11,12] These drawbacks can be prevented by affinity binding, where the carrier interacts with a specific group in the enzyme without affecting the enzymatic activity.[22] Affinity binding allows for carrier reuse through reversible attachment to the support.[22,23] One example of affinity binding is adapted from immobilized metal affinity chromatography (IMAC), a protein purification method.[24–26] It is based on the interaction between a polyhistidine tag (His-Tag) in the enzyme and a metal ion coordinated to the carrier via a chelating ligand, mostly nitrilotriacetic acid (NTA).[12,21,26] Microgels containing NTA have been fabricated and used as carriers for enzymes and proteins in a few studies before.[23,27–29] In contrast to previous studies, our approach involves the synthesis of smaller, shell-functionalized microgels.[30] This design enhances the surface-to-volume ratio and facilitates the accessibility of NTA units for the immobilization of *Pm*HAS.

Only a limited number of research articles have previously been published on the immobilization of *Pm*HAS.[4,6,31,32] Qiao et al.[4] successfully immobilized His_6-tagged *Pm*HAS on metal-organic frameworks. However, their study focused solely on quantifying the conversion of HA monomers to the respective disaccharide, without exploring the quantification of HA polysaccharide formation. Mori et al.[32] immobilized *Pm*HAS on a mica surface, focusing on the development of a visualization technique. Furthermore, DeAngelis et al.[31] mutated *Pm*HAS to produce two single-action enzymes, which were immobilized on agarose beads for the synthesis of specific oligosaccharides. Gottschalk et al.[6] demonstrated the immobilization of His_6-tagged *Pm*HAS on NTA-bearing magnetic particles via affinity binding, while maintaining enzymatic activity. In this study, the focus is shifted from using hard magnetic particles[6] to developing a soft microgel carrier capable of reversibly immobilizing *Pm*HAS. Unlike the previously utilized magnetic beads[,6] the biocompatibility of NTA-functionalized poly(*N*-vinylcaprolactam) (pVCL)-based microgels has been demonstrated, allowing their use in biological applications.[30] Moreover, future efforts to scale up the synthesis of our developed microgels should enable the production of larger quantities of HA to meet widespread demand, whereas the magnetic beads are intended for small-scale production only. Furthermore, we propose that utilizing microgels as carriers can enhance *Pm*HAS productivity, leveraging the advantages of microgels over other nanocarriers, and aiding in improved enzyme loading efficiency and substrate diffusion.

To summarize, this work utilizes pVCL-based core–shell microgels with an NTA-rich shell[30] to immobilize His_6-tagged *Pm*HAS. The immobilized *Pm*HAS is characterized in terms of its enzymatic activity and its ability to form high molecular weight HA.

2. Results and Discussion

2.1. Synthesis and Fundamental Characterization of Microgels

Poly (*N*-vinylcaprolactam-2,2′- ((5-acrylamido-1-carboxypentyl) azanediyl)diacetic acid) (p(VCL/NTAaa)) microgels were successfully synthesized according to the semi-batch synthesis developed in our previous work.[30] The synthesis procedure is depicted in **Scheme 1**.

The polymerization of VCL and the crosslinker BIS is initiated by the addition of AMPA. Due to the high reactivity of BIS,[33] a highly cross–linked BIS- and VCL-rich core is formed initially. After 30 s, the addition of NTAMaa, dissolved in DMSO, is started. This addition causes a slowdown of the overall reaction, accompanied by a relatively slow reactivity of NTAMaa.[30]

Thus, the decreasing reactivity from BIS and VCL to NTAMaa, combined with the semi-batch polymerization technique, results in the formation of an NTAMaa-rich shell after most of BIS and VCL have already reacted. The crosslinking density is highest in the microgel core.

The theoretical and actual NTA contents are shown in **Table 1**. The corresponding FT-IR spectra are shown in Figures S3 and S4 (Supporting Information). Due to the low height of the peak of the C=O vibration of the carboxylic acid groups of NTA, only NTA concentrations above 1 mol% could be investigated regarding their actual comonomer content. The experimental results in Table 1 indicate that incorporated NTA amounts match the expected values with low deviations. In the following, p(VCL/NTAaa) are referenced with their theoretical NTA amounts for concentrations up to 1 mol% and with their actual NTA amounts for concentrations above 1 mol%. All NTA concentrations are titled χ_{NTA}.

The microgels were further analyzed using ELS and DLS measurements (Table 1). Due to the strong acidity of NTA, the dilute dispersions used for ELS and DLS measurements at higher NTA contents in p(VCL/NTAaa) reached pH values below the pH of the used H_2O (pH 6). The hydrodynamic diameters of the microgels at 25 °C show varying sizes between 349 and 759 nm. The evaluation of the polydispersity index (PDI) obtained from DLS indicates the formation of monomodal samples with a reasonably narrow size distribution. Upon examining the microgel sizes, a clear increase is observed from the microgels containing χ_{NTA} = 0.1 mol% to those containing χ_{NTA} = 1 mol%. This phenomenon is explained by the repulsion of the negatively charged

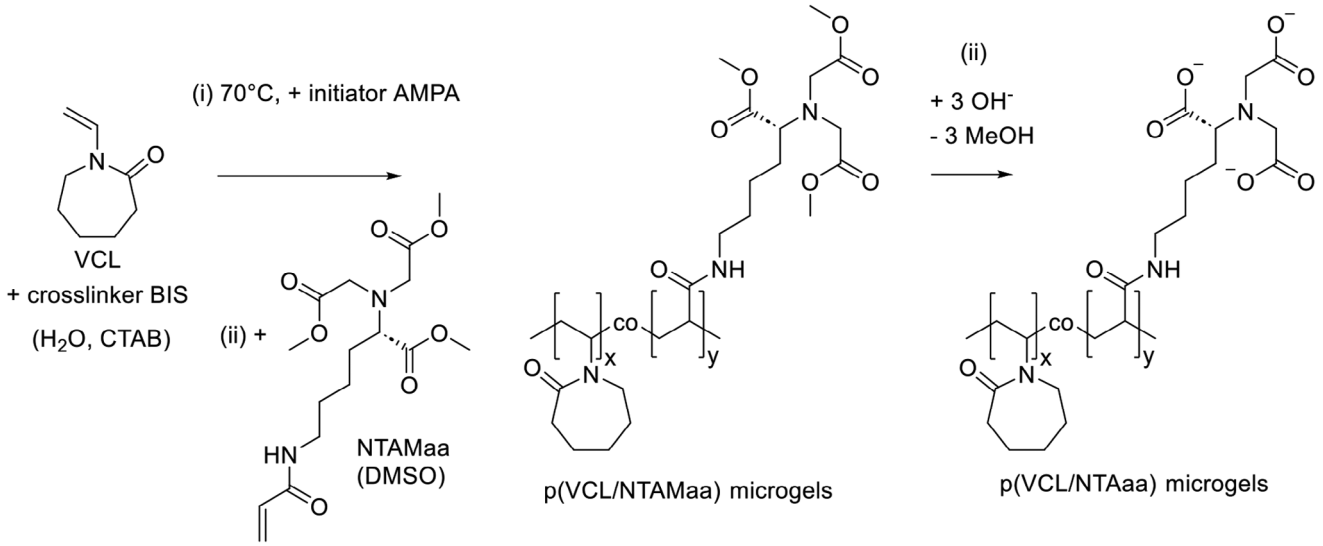

Scheme 1. Semi-batch precipitation polymerization of p(VCL/NTAaa) microgels.[30] The monomer VCL is dissolved in water along with the crosslinker BIS and the surfactant CTAB. i) The reaction is initiated by heating the mixture to 70 °C, followed by the addition of the initiator AMPA. The microgel core starts forming, containing VCL cross–linked by BIS. ii) Subsequently, the comonomer NTAMaa (dissolved in DMSO) is slowly added utilizing a syringe pump. Due to the lower reactivity of NTAMaa compared to VCL, most VCL reacts first. iii) After cooling down to room temperature, the resulting p(VCL/NTAMaa) microgels are treated with NaOH to hydrolyze the ester and expose the carboxylic groups. The p(VCL/NTAaa) microgels are purified through dialysis. Due to the delayed addition and the low reactivity of NTAMaa, the microgels possess a VCL- and BIS-rich core and an NTAaa-rich shell.

Table 1. Zeta potential (ζ), hydrodynamic diameter (D_h), and PDI of p(VCL/NTAaa) microgels synthesized with different amounts of NTA ($\chi_{NTA,theor}$). The actual NTA content ($\chi_{NTA,actual}$) was determined using FT-IR spectroscopy while ζ, D_h, and PDI were determined using ELS (ζ) and DLS (D_h, PDI) measurements at $T = 25$ °C with scattering angles of $\theta = 90°$ (DLS) and $\theta = 12.8°$ (ELS) in H_2O. Yields of the microgel synthesis were determined gravimetrically.

$\chi_{NTA,theor.}$ [mol%]	$\chi_{NTA,actual}$ [mol%]	ζ [mV][a]	D_h [nm][a]	PDI [a.u.][a]	Yield [%]
0 [d]	0	3.2 ± 0.2[b]	576 ± 15[b]	0.086 ± 0.051[b]	83
0.1	-	-6.0 ± 0.7[b]	349 ± 10[b]	0.080 ± 0.027[b]	72
0.25	-	-10.2 ± 1.1[b]	451 ± 23[b]	0.119 ± 0.043[b]	69
0.5 [d]	-	-18.0 ± 1.3[b]	584 ± 20[b]	0.132 ± 0.035[b]	68
1	-	-21.3 ± 1.2[c]	644 ± 24[c]	0.143 ± 0.019[c]	58
2	1.9	-25.7 ± 0.4[c]	759 ± 55[c]	0.283 ± 0.013[c]	74
2.5 [d]	2.2	-38.4 ± 0.2[c]	640 ± 11[c]	0.147 ± 0.018[c]	85

[a] The dilute p(VCL/NTAaa) dispersion (0.5 mg mL^{-1}) prepared for ELS and DLS measurements resulted in a neutral pH at low NTA contents ($\chi_{NTA,actual} = 0.1$ to 0.5 mol%) and in a slightly acidic pH of 5 at higher NTA contents ($\chi_{NTA,actual} = 1$ to 2.2 mol%); [b] pH 6, the pH corresponds to the pH of the used HPLC water; [c] pH 5. [d] characterization results of marked microgels have been previously reported[30] but are listed here for comprehensiveness.

NTA groups from each other and the associated higher degree of swelling. However, at higher χ_{NTA}, no clear trend was established aligning with our previous results where no distinct correlation of size and comonomer amount was found.[30] This effect could be explained by variations in the microgel morphology. Grabowski et al.[34] have previously shown that the amount of comonomer used in reaction, can influence the microgel shape, and such an effect was confirmed for the used comonomer NTAMaa in our previous study.[30] NTAMaa, being the esterified and much more hydrophobic version of NTAaa, has a strong influence on microgel morphology, which can itself impact microgel size.

At low NTAaa concentrations, zeta potential measurements could be used as a qualitative indication of the comonomer content. Due to the use of a semi-batch method, the COOH groups of NTA should be located in the microgel shell. Their strong acidity would thus lead to a negative surface potential which decreases with increasing NTAaa incorporation. As expected, a strong decrease in the zeta potential is visible in the shown range of χ_{NTA} (Table 1).

To summarize, we were able to synthesize microgels with a relatively narrow size distribution containing different amounts of comonomer χ_{NTA}.

2.2. Incorporation of Metal Ions into p(VCL/NTAaa) Microgels

After the successful fabrication and characterization of p(VCL/NTAaa) microgels, they were used for the incorporation of metal ions via complexation to enable enzyme immobilization by metal affinity binding. This was achieved by adding a highly concentrated metal salt solution to the microgels followed by the dialysis to remove non-complexed metal ions. The binding of the carboxylic groups of NTA with the metal ions results in the formation of a complex, primarily driven by electrostatic interactions.[35] Due to the additional binding of the amine group, NTA serves as a tetradentate ligand.[35,36] However, it has been shown that for alkaline earth metals (Mg^{2+}), NTA only serves as a tridentate ligand,[37] reducing the binding strength due to the lower chelate effect. The incorporation of Ni^{2+}, Co^{2+}, Mn^{2+}, Mg^{2+}, and Fe^{2+} into p(VCL/NTAaa) microgels with $\chi_{NTA} = 1$ mol% was verified via inductively coupled plasma optical emission spectroscopy (ICP-OES). The amount of metal in each

Table 2. Metal content of different p(VCL/NTAaa@Mt) samples after incorporation of different metal (Mt) ions determined by ICP-OES; the amount of occupied NTA coordination sites; microgel yields after the metal ion incorporation as determined gravimetrically. The last column shows the metal concentration in dispersions of p(VCL/NTAaa@Mt) samples at microgel concentrations of 3 mg mL^{-1}.

Metal ion	Metal content [mg g^{-1}]	Metal content [µmol $mmol^{-1}$]	Occupied NTA sites [%]	Yield [%]	Metal concentration [mM]
Ni^{2+}	3.9	9.3	96	74	0.20
Co^{2+}	3.6	8.0	82	99	0.17
Mn^{2+}	1.6	4.1	42	93	0.09
Mg^{2+}	0.5	2.8	28	87	0.06
Fe^{2+}	(59.7)[a)]	(131.3)[a)]	(1347)[a)]	(111)[a)]	3.21

[a)] Fe^{2+} ions have shown to strongly interact not only with NTA units in p(VCL/NTAaa) but also with VCL, leading to a far exceeded Fe incorporation.

microgel sample as well as the amount of occupied NTA groups are shown in **Table 2**. For the calculation of the amount of occupied NTA groups, it is assumed that one NTA group binds one metal ion. Furthermore, Table 2 shows the attained yields of microgels after the metal ion incorporation, determined by gravimetry.

According to ICP-OES results, all microgel samples contain the desired metal ions. Regarding the loading efficiency into the microgels, Ni^{2+} and Co^{2+} seem to be the most suitable metal ions as 82% (Co^{2+}) to 96% (Ni^{2+}) of all NTA groups are occupied. The amount of coordinated metal ions for Mn^{2+} (42%) and Mg^{2+} (28%) is lower so it is expected that these ions are less suitable for this application. These results align with the formation constants of NTA complexes reported in the literature:[38,39] the strongest NTA@Mt complex is formed with Ni^{2+}, followed by Co^{2+}. The use of Mn^{2+} and Mg^{2+} leads to the formation of weaker complexes. The yields of the metal ion incorporation are between 74% and 99% depending on how well the microgel solution could be transferred into the dialysis tubes. For Ni^{2+} strong aggregations of the microgels occurred during metal loading due to the strong interaction of the microgels in the highly concentrated metal salt solution. This explains the slightly lower yield of 74%. All beforementioned samples formed a homogeneous dispersion after the complete removal of the metal salts in solution by dialysis. Furthermore, the resulting lyophilized p(VCL/NTAaa@Mt) microgels had an appearance similar to the p(VCL/NTAaa) microgels: homogeneous white powder, slightly blueish for immobilized Ni^{2+} and slightly orange for immobilized Fe^{2+}.

It is noticeable that the amount of Fe in the microgel is more than 10 times higher than the maximum number of binding sites supplied by NTA. Furthermore, the yield of the ion incorporation is above 100% indicating that more than the desired amount of metal ions was found in the sample. It was further observed that the obtained p(VCL/NTAaa@Fe) microgels showed an inhomogeneous appearance after lyophilization showing rather brownish parts and parts that were less colored. This indicates that next to the white microgel powder, metal salts are contained in the sample. It is postulated that the Fe^{2+} ions strongly interact with the microgel in dispersion and are thus not removed by dialysis. The brownish color further indicates that Fe^{2+} has been partially oxidized to form Fe^{3+}. The color change from green to yellow during metal ion incorporation further undermines the change in the oxidation state. The large amount of Fe in the sample shows that the interaction cannot only be caused by the formation of Fe-NTA complexes. These results indicate that Fe^{2+} may not be suitable for loading into microgels by complexation with NTA. To further investigate these interactions of pure pVCL microgel with metal ions (Ni^{2+}, Co^{2+}, Mn^{2+}, Mg^{2+}, Fe^{2+}), the immobilization process was repeated for a pVCL microgel without added NTA comonomer. The results are shown in Figure S5 (Supporting Information) and confirm that interactions between the microgel network and Fe ions lead to the uptake of high amounts of Fe. The content of all other metal ions in p(VCL@Mt) microgels is nearly negligible, significantly lower than observed in p(VCL/NTAaa@Mt) microgels. Further information regarding this comparison can be found in the Supporting Information.

The p(VCL/NTAaa@Mt) microgels were further investigated via zeta potential and DLS measurements. Due to the incorporation of positively charged metal ions, the zeta potential increases when comparing p(VCL/NTAaa@Mt) to the initial p(VCL/NTAaa) microgels. The detailed characterization results are found in Figures S6 and S7 in the Supporting Information.

Finally, p(VCL/NTAaa@Ni) microgels containing different comonomer contents χ_{NTA} were compared to the previously synthesized p(VCL/NTAaa) regarding their morphology using AFM imaging (**Figure 1**; Figure S8 Supporting Information).

To acquire AFM images, the microgels were spin-coated onto plasma-activated Si wafers and subsequently dried. AFM imaging yielded height profiles, where darker colors represent the Si wafer background, while lighter colors indicate the adsorbed microgels. The adsorbates are thereby depicted in a brown-to-white color scale based on their height relative to the surface. Due to the soft nature of the adsorbed microgels, they can deform upon adsorption on a surface, typically spreading across the surface of the Si wafer. This allows for the visualization of core–shell structures, where the denser network structures in a highly cross–linked, more rigid core exhibit greater height. In contrast, the microgel shell possesses a softer, loosely non-cross–linked structure. The resulting core–shell morphology, often observed at interfaces, is typically referred to as a "fried egg" structure.[40,41]

The images found in Figure 1 and Figure S8 (Supporting Information) all show relatively monodisperse p(VCL/NTAaa) microgels with a slightly higher polydispersity for $\chi_{NTA} = 1.9$ mol% as visible in Figure S8 (Supporting Information). This sample also possesses a higher PDI as shown in DLS results. In Table S1 (Supporting Information), we list the diameters obtained from AFM images of adsorbed p(VCL/NTAaa) microgels in the dried state (D_{AFM}) compared to the hydrodynamic diameter (D_h) of microgels obtained through DLS measurements. Additionally, the D_{AFM}/D_h ratio is provided for enhanced comparison, revealing potential correlations between the individual diameters.

At very low χ_{NTA} (0.1 to 0.25 mol%), the dried microgels possess ≈50% of the size of the swollen microgels, similar to pure pVCL microgels. This indicates that the comonomer has not yet strongly altered the microgel properties and the microgels spread similarly across the surface. However, as χ_{NTA} increases to intermediate values (0.5 to 1.9 mol%), a decrease in D_{AFM}/D_h (32% to 22%) is observed. This decrease is caused by both an increase in D_h and a reduction in D_{AFM}. The increase in D_h can be attributed

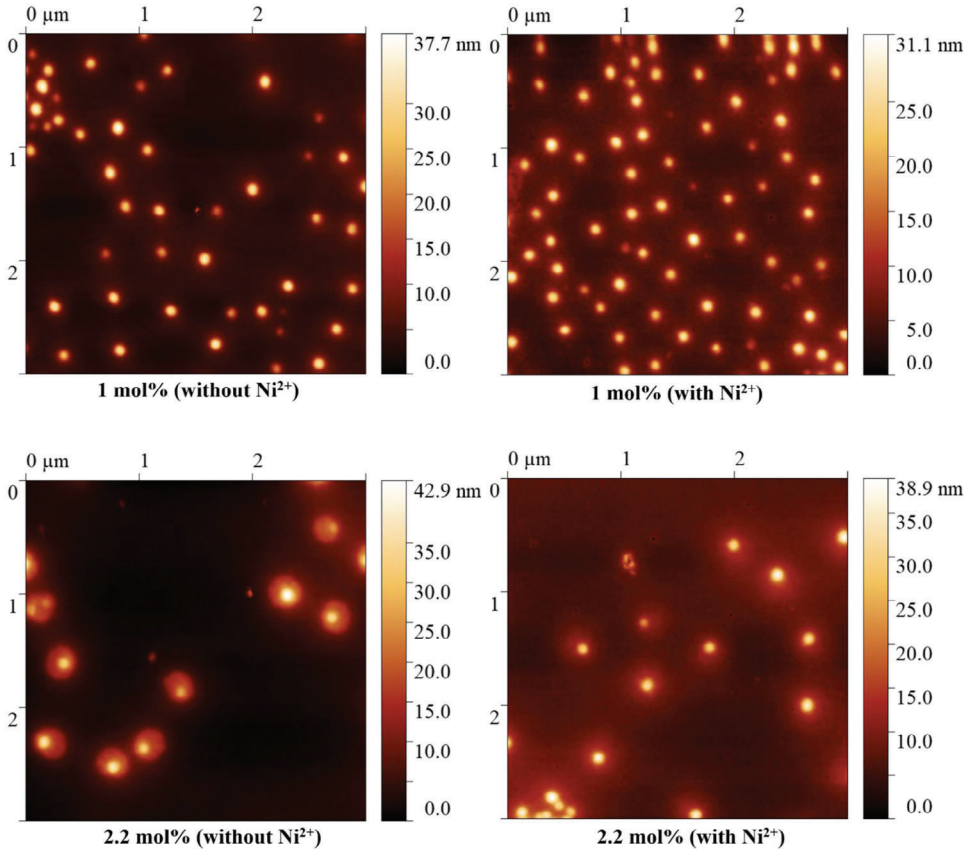

Figure 1. AFM images (height profiles) for p(VCL/NTAaa) containing comonomer contents χ_{NTA} of 1 and 2.2 mol% and the corresponding p(VCL/NTAaa@Ni) microgel. The colors within the AFM images represent the height of the microgels, starting from the Si wafer base at 0 nm height. The corresponding height values can be found in the legends. The image of p(VCL/NTAaa) with $\chi_{NTA,theor}$ = 2.2 mol% (without Ni^{2+} (bottom left) is reprinted with permission from reference.[30] Copyright 2024 American Chemical Society (ACS).

to the increased comonomer content along with the repulsion of the negatively charged NTA groups from each other, leading to a higher degree of swelling. This emergence of the NTAaa-rich microgel shell is not visibly discernible in AFM. However, upon closer examination, the boundaries of the microgel are less distinct: The microgel core, possessing the largest height merges into fuzzy, flat outer layers, representing the thin shell. Possibly, the outermost dangling chains are too thin to be visualized. At these χ_{NTA} (0.5 to 1.9 mol%), D_{AFM} represents the microgel core, rather than the full microgel. When increasing χ_{NTA} even more (χ_{NTA} = 2.2 mol%), the dried microgels show ≈60% of the size of the swollen microgels. This aligns with previous findings[30] and is explained by most of the hydrophilic shell now being measurable due to its increased volume. The NTAaa-rich shell spreads across the surface, resulting in an increased recorded D_{AFM} of the dried microgels.

To summarize, we can observe microgels without a strongly visible shell for χ_{NTA} of 0.1 mol% to 1 mol% while the microgels containing 1.9 mol% NTA have a fuzzy morphology, and microgels containing 2.2 mol% show a clear core–shell behavior. The morphology of these microgels has been thoroughly discussed in our previous publication[30] and is explained by the strong influence of the comonomer NTAMaa during copolymerization. Due to the lower reactivity of NTAMaa compared to the main comonomer VCL and the crosslinker BIS, it is primarily incorporated into the microgel shell at all concentrations of χ_{NTA}.[30] Although not readily visible in AFM at low χ_{NTA}, the NTAaa-rich shell becomes apparent at higher χ_{NTA} due to its increased thickness. At higher amounts of χ_{NTA}, the change in morphology may not only influence the overall size of the microgels and the visibility of the microgel shell but also their shape. During polymerization, NTAMaa units exhibit strong interactions with each other due to hydrophobic forces. This interaction can result in the self-assembly of these groups, contributing to the formation of a slightly asymmetric structure, which, in turn, can cause variations in size.[30,34] Such an asymmetric structure is visible for microgels with χ_{NTA} = 2.2 mol%.

When comparing p(VCL/NTAaa) to the corresponding p(VCL/NTAaa@Ni) microgels, the samples containing 0.1 mol% to 1 mol% NTA do not show visible changes regarding their size and morphology. The microgels containing 2.2 mol% NTA (Figure 1) show a reduced shell height, which can also be explained by a decreased electrostatic repulsion of the carboxylic acid groups. These results are consistent with the previously obtained data.

The core–shell structure of the obtained microgels is particularly important for enzyme immobilization: This design not only enhances the accessibility of NTAaa units for the immobilization

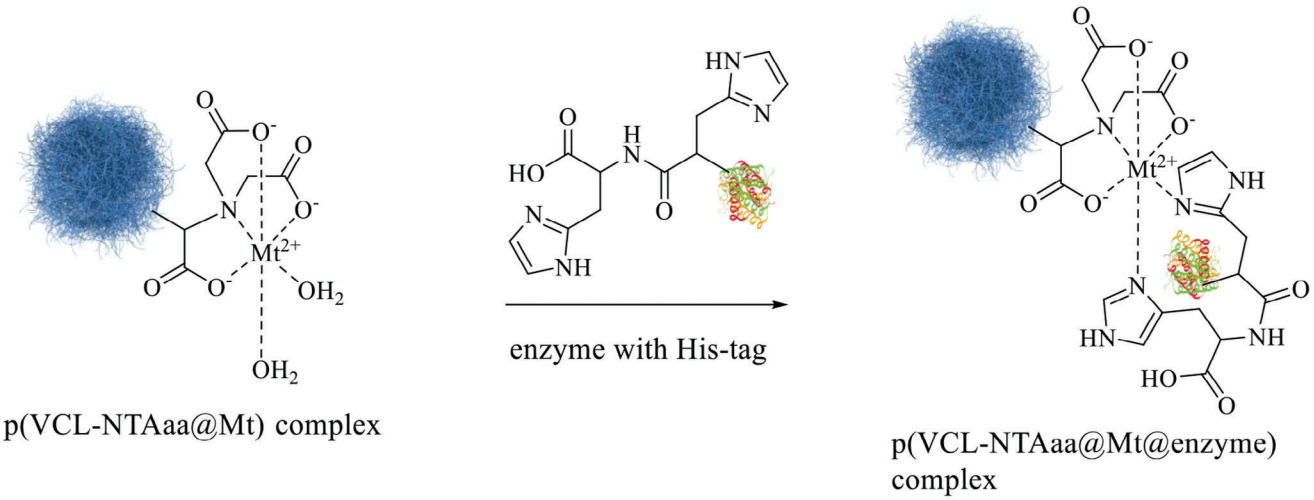

Scheme 2. Schematic depiction of the immobilization of an enzyme via metal affinity binding on NTA@Mt-based microgel support, here p(VCL/NTAaa@Mt). The complex is depicted in the desired octahedral geometry of NTA@Mt, supplying two free coordination sites for the enzyme.

of *Pm*HAS but also improves the diffusion of enzyme substrates and products to and from *Pm*HAS during the enzymatic synthesis of HA. Simultaneously, the microgel core maintains the overall stability of the microgel and facilitates the simplified separation of the microgel from enzymatic products. In the following section, we will delve into the immobilization of *Pm*HAS onto these microgels.

2.3. Fabrication and Characterization of Enzyme-Microgel Hybrids

The goal of this research is the fabrication of an active p(VCL/NTAaa@Mt@*Pm*HAS) enzyme-microgel hybrid, based on the work of Gottschalk et al.[6] where His Mag Sepharose Ni beads were used for the immobilization of His_6-tagged *Pm*HAS. The use of pVCL-based microgels as a carrier offers an alternative to magnetic beads with the potential for a synthesis scale-up. Furthermore, our objective is to increase the overall yield of HA. We hypothesize that employing microgels as carriers can enhance PmHAS productivity. The magnetic beads, according to the supplier, are relatively dense, whereas microgels offer greater porosity, providing a distinct advantage for the molecular transport of reagents. Additionally, magnetic beads are prone to sedimentation, potentially leading to uneven distribution of the catalytic carrier and hindering HA production. Additionally, the use of the microgels in biomedical applications is enabled: In our previous work, we have shown that not only pVCL microgels but also p(VCL/NTAaa) are biocompatible, especially at χ_{NTA} below 2.2 mol%.[30] Within the present work, the His_6-tagged enzyme *Pm*HAS was incorporated into p(VCL/NTAaa@Mt) microgels via metal affinity binding. To supply two free coordination sites for the enzyme, the complex should be preferably in octahedral geometry with a coordination number of six, as depicted in Scheme 2. The complex geometry however strongly depends on the used metal ion and its electron shell leading to varying orbital hybridization,[36] and alone the attained geometry will influence the enzyme immobilization on p(VCL/NTAaa@Mt) microgels: if the coordination number is lower than 6, there may be a lower amount of free coordination sites for the enzyme. It has been reported in the literature[42–44] that NTA@Ni^{2+} and NTA@Co^{2+} complexes possess an octahedral structure in the form of [Mt-(NTA)$(H_2O)_2$] as depicted in Scheme 2. For Mn^{2+}, Zetter et al.[45] have postulated a non-octahedral structure with a coordination number higher than 6. While the exact structure could not be determined, the coordination number indicates free coordination sites for the enzyme. According to the literature, Fe^{2+} most likely oxidizes to form six-coordinate Fe^{3+} complexes with NTA such as distorted octahedral structures.[46,47] Mg^{2+} is expected not to form stable complexes with NTA due to its small size[48] and coordination of NTA as a tridentate ligand only.[37] Given the low binding strength, we anticipate only minimal binding to *Pm*HAS independent of the complex geometry.

The formed hybrid microgels are compared concerning their enzyme content. For this, the amount of non-incorporated enzymes was determined through a Bradford assay, enabling the calculation of the enzyme content in enzyme-microgel hybrids. Furthermore, the hybrid microgels are compared regarding their activity by comparison of the formed UDP amount after defined periods. The enzyme *Pm*HAS forms HA from the two UDP-sugars UDP-GlcNAc and UDP-GlcA as shown in Scheme S1 in the Supporting Information. During this reaction UDP is formed, providing an ideal measure for the performance of the p(VCL/NTAaa@Mt@*Pm*HAS) hybrids. Therefore, we used capillary electrophoresis (CE) for the measurement of the UDP concentration.

Different parameters were varied to improve the performance of p(VCL/NTAaa@Mt@*Pm*HAS). First, different metal ions (Ni^{2+}, Co^{2+}, Mn^{2+}, Mg^{2+}, and $Fe^{2+/3+}$) were compared regarding their influence on the performance of the microgel enzyme hybrid. After choosing Ni^{2+} for further experiments, the concentration of NTAaa within p(VCL/NTAaa@Ni@*Pm*HAS) microgels and thus of complexed Ni^{2+} was varied. The quantity of the purified enzyme was then increased for hybrid microgels with fixed NTAaa contents to enable the occupation of all free NTAaa@Ni coordination sites. Finally, one major advantage of enzyme im-

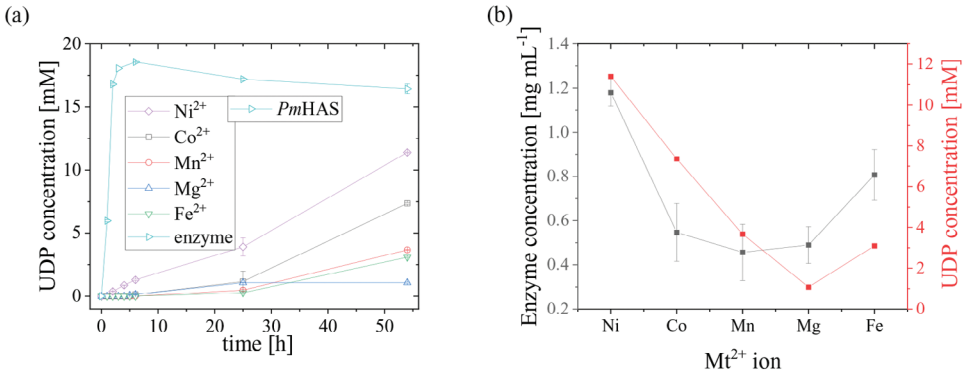

Figure 2. a) p(VCL/NTAaa@Mt@PmHAS) samples with χ_{NTA} = 1 mol% containing different metal ions (Ni^{2+}, Co^{2+}, Mn^{2+}, Mg^{2+}, and $Fe^{2+/3+}$) were investigated regarding the UDP formation over time. A concentration of 1.5 mg mL^{-1} purified PmHAS was used for enzyme immobilization. This corresponds to ≈3.78 available coordination sites in the hybrid microgel (two per NTA unit) to His groups in the His_6-Tag of PmHAS. The microgel samples are compared to purified His_6-tagged PmHAS (1.5 mg mL^{-1}). b) Formed UDP after 54 h of reaction time is compared to the amount of immobilized enzymes as obtained through a Bradford assay.

mobilization is the facilitation of enzyme recycling. Therefore, in the final step, the reuse of p(VCL/NTAaa@Ni@*Pm*HAS) was tested for three cycles of HA formation.

2.3.1. Variation of the Used Cation

After the incorporation of Ni^{2+}, Co^{2+}, Mn^{2+}, Mg^{2+}, and $Fe^{2+/3+}$ into p(VCL/NTAaa) microgels, as described previously, the resulting p(VCL/NTAaa@Mt) were used for the incorporation of *Pm*HAS. Due to the previously determined metal loading efficiency, the highest *Pm*HAS binding could be expected by hybrid microgels complexing Ni^{2+} and Co^{2+}, followed by Mn^{2+} and Mg^{2+}. However, we have to consider, that not only the amount of metal plays an important role but also other factors such as complex stability and the affinity of the enzyme to the metal complex. The enzymes' affinity for Ni^{2+} and Co^{2+} is known to be established through the His_6Tag.[26,49] In the case of Mn^{2+}, Mg^{2+}, and $Fe^{2+/3+}$, it remains unclear whether binding is mediated by the His_6Tag or other amino acid residues. Furthermore, Mn^{2+} and Mg^{2+} are cofactors of *Pm*HAS and are complexed by the UDP-sugars to obtain active substrates, which may interfere with the affinity binding of the enzyme. The behavior of p(VCL/NTAaa@Fe) cannot be predicted due to strong interactions of $Fe^{2+/3+}$ with the contained VCL units.

The enzymatic synthesis of HA over time is monitored via the UDP concentration for different p(VCL/NTAaa@Mt@*Pm*HAS) which is shown in **Figure 2a**.

The observation of the UDP concentration over time shows a slower UDP formation, and therefore HA synthesis, for all p(VCL/NTAaa@Mt@*Pm*HAS) hybrids if compared to the pure enzyme. Different factors can lead to this decrease in the reaction rate. Firstly, steric hindrance in the microgel can lead to the reduction of enzyme activity and consequently slower formation of HA. The enzymes are not only located in very close proximity to each other but also the polymer chains could lead to steric effects when the HA polymer is formed. Furthermore, full immobilization is not guaranteed so the enzyme concentration in p(VCL/NTAaa@Mt@*Pm*HAS) is lower than in the *Pm*HAS solution (data discussed below).

When observing the UDP concentration in the purified *Pm*HAS sample, we see a fast increase to 18.6 mM which is 93% of the maximum possible UDP concentration of 20 mM, however, followed by a slow decrease to 16.4 mM (82%). This can be explained by the hydrolysis of UDP in the alkaline environment to form UMP and phosphate as shown in Scheme S2 in the Supporting Information. Previous works have shown that UMP forms during the synthesis of HA from *Pm*HAS.[50,51]

When comparing the p(VCL/NTAaa@Mt@*Pm*HAS) hybrids according to their attained UDP concentration, it is noticeable, that the rates go very well with the previously determined metal ion concentration. The highest UDP concentration after 54 h was achieved by hybrid microgels containing Ni^{2+} (57% of the maximum yield), followed by Co^{2+} (37%). The results for p(VCL/NTAaa@Mt@*Pm*HAS) containing Mn^{2+} (18%), $Fe^{2+/3+}$ (16%), and Mg^{2+} (5%) are lower. The yield of microgels containing $Fe^{2+/3+}$ indicates that the NTA units were at least partially available for the complexation of the enzyme. However, there is still no indication of the amount of NTAaa@Fe. Next to the amount of immobilized metal, the presence of free metal ions may influence the *Pm*HAS activity as previously shown in the work of Eisele et al.[51] According to their work, the presence of Ni^{2+} leads to an almost complete deactivation of *Pm*HAS, however, this was investigated for concentrations of 1 mM and higher. In our system, the present Ni^{2+} concentration is 0.2 mM lower, as shown in Table 2. Furthermore, the comparability to the Ni^{2+} in our system is limited because it is complexed by NTA and most likely possesses a different behavior compared to free metal ions. Even so, a deactivating effect could be present even at lower concentrations.

We are also comparing the concentration of UDP formed after 54 h to the amount of enzymes in the microgels (Figure 2b). Furthermore, we are comparing the *Pm*HAS concentration in the samples to the metal ion concentration in Figure S9 (Supporting Information) for clarification of a possible relationship. Most enzymes were incorporated with Ni^{2+}, as expected, while the other metal ions led to lower amounts of metal incorporated. The second highest number of enzymes was bound through Fe^{2+}, but the resulting UDP formation is not as high. The previously described extremely high concentration of $Fe^{2+/3+}$ in the

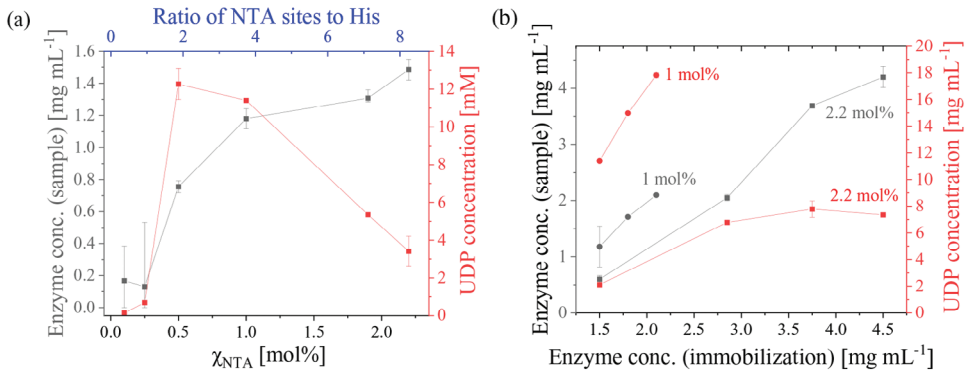

Figure 3. Enzyme-microgel hybrids were investigated regarding their incorporated enzyme amount (left Y axis) and the amount of formed UDP after 54 h of reaction time (right Y axis) as obtained from Bradford and CE measurements, respectively. a) p(VCL/NTAaa@Ni@PmHAS) samples are investigated regarding their dependence on χ_{NTA} and thus of Ni^{2+}. A concentration of 1.5 mg mL^{-1} purified PmHAS was used for enzyme immobilization. A second x-axis is used to show the ratio of available coordination sites in the hybrid microgel to His groups in the His_6-Tag of PmHAS. b) Comparison of p(VCL/NTAaa@Ni@PmHAS) samples that were prepared with varying PmHAS amounts. Hybrid microgels of two different amounts of NTA (χ_{NTA} = 1 and 2.2 mol%) are compared. The data point for χ_{NTA} = 1 mol% and the enzyme concentration of 2.1 mg mL^{-1} was taken after 24 h instead of 54 h.

microgels could, therefore while enabling *Pm*HAS immobilization, disturb its activity. Due to the nonspecific interactions of $Fe^{2+/3+}$ with the microgels, the use of $Fe^{2+/3+}$ is not recommended. Co^{2+} shows slightly lower immobilization, which was not expected due to the high Co^{2+} content and enzyme activity. Therefore, the immobilized *Pm*HAS enzyme may be more active but present in a lower concentration. Mn^{2+} and Mg^{2+} show the lowest amount of *Pm*HAS, which agrees with the low metal contents. Overall, the Bradford measurements show relatively large standard deviations, which may be explained by the presence of single microgels in the supernatant. The microgels could disturb the UV–Vis measurements as the present microgels are UV–Vis active compounds[30] and interactions between the Bradford reagent and the microgels could slightly distort the results.

Summarizing, the results indicate that p(VCL/NTAaa@Ni) is the most suitable hybrid microgel for the immobilization of *Pm*HAS and the production of HA. Therefore, further studies are conducted to optimize the enzymatic activity. To enable the immobilization of the optimal amount of enzyme, the NTAaa amount within the microgel is varied, associated with a changing Ni^{2+} amount.

2.3.2. Variation of the Ni-NTA Content

Microgels with varying amounts of NTAaa were synthesized and used for incorporation for Ni^{2+} and immobilization of *Pm*HAS. They were then investigated regarding their enzymatic action by comparison of the UDP amount formed after certain periods. The full measurements containing data points at different times are found in Figure S10 (Supporting Information). For better comparability, the UDP concentration formed after 54 h of enzymatic reaction is shown in **Figure 3a**, compared to the enzyme concentration in the enzyme-microgel hybrids.

When analyzing the data, we observe an increasing enzyme concentration in the samples with increasing χ_{NTA}, as the amount of comonomer determines the number of available binding sites for *Pm*HAS at a fixed enzyme concentration of 1.5 mg mL^{-1} purified *Pm*HAS for loading. Consequently, with increasing enzyme content, the UDP concentration increases from low NTA concentrations (χ_{NTA} = 0.1 or 0.25 mol%) to higher comonomer contents (0.5 mol%). However, at higher χ_{NTA}, a decrease in the UDP concentration is observed instead of a further increase. To further investigate this effect, we included the ratio of available coordination sites in the microgel (two per NTA unit) to the six His groups in the His_6-Tag of *Pm*HAS in the graph. The calculated ratio for each of the microgels is found in Table S2 in the Supporting Information. As shown in Figure 3a, for χ_{NTA} = 0.25 mol% the number of coordination sites could be sufficiently high to bind all His groups in the His_6-Tag. Even so, the amount of incorporated enzymes is still relatively low. That indicates that not all His groups can bind simultaneously to p(VCL/NTAaa@Ni) which is consistent with the high steric requirements: if all six His groups are bound, three NTA groups need to be in very close proximity to each other, and the enzyme. Moving to hybrid microgels with a slight excess of available coordination sites (χ_{NTA} = 0.5- 1 mol%), the *Pm*HAS concentration in microgels can be immensely increased, which also leads to a further activity increase. While the enzyme concentration further increases, the ability of the hybrid to form UDP declines. This can be once more explained by observing the ratio of NTA coordination sites to the number of His groups in the His_6-Tag of *Pm*HAS. For larger NTA concentrations (χ_{NTA} = 1.9-2.2 mol%), the ratio is quite large, leaving a high number of free coordination sites, even if all enzymes are bound to the microgel hybrid via the His_6-Tag. This can lead to unwanted interactions of NTA with His groups beyond the His_6-Tag, as *Pm*HAS contains a sum of 23 His groups (including the His_6-Tag) in the enzyme as can be seen in the amino acid sequence shown in the Supporting Information. The interaction can lead to a deactivation of the enzyme, especially for His groups located in the active center.

These results show, that a suitable ratio of NTA coordination sites to His groups in the His_6-Tag could be important. Besides the variation of the NTA concentration, this ratio can also be affected by the enzyme concentration. Thus, in a further step, the enzyme concentration was varied.

2.3.3. Variation of the Enzyme Amount During Immobilization

The previous results indicate, that a suitable ratio of NTA groups to enzymes is needed for sufficiently high UDP synthesis. In this way, adverse interactions of NTA with His groups of *Pm*HAS can be minimized while still enabling the immobilization of a large enzyme amount via the His_6-tag. Previously, the p(VCL/NTAaa@Ni@*Pm*HAS) hybrid microgel containing χ_{NTA} = 2.2 mol% did not show high enzymatic activity. However, an increase in the *Pm*HAS amount could lead to an improvement of the system by the presence of fewer deactivating interactions and simply more enzymes in the system. Furthermore, the microgel containing χ_{NTA} = 1 mol% was used to compare the effects of an increased *Pm*HAS amount and to enable further optimization of the p(VCL/NTAaa@Ni@*Pm*HAS) system. Unlike the hybrid microgel containing χ_{NTA} = 0.5 mol% NTA, this microgel still possesses a high amount of available NTA sites for the immobilization of *Pm*HAS, so an increase in the enzyme concentration should also lead to a higher UDP synthesis. The UDP amounts formed by p(VCL/NTAaa@Ni@*Pm*HAS) after certain periods are shown in Figure S11 in the Supporting Information. For better comparability, the formed UDP amounts after 54 h are shown in Figure 3b, compared to the enzyme concentration in the samples. The only exception here is the data point for p(VCL/NTAaa@Ni@*Pm*HAS) with χ_{NTA} = 1 mol% and an enzyme concentration of 2.1 mg mL^{-1} which was taken at 24 h. Even though a shorter reaction time was used, the expected activity increase can already be seen for this data point.

With increasing enzyme concentration, the p(VCL/NTAaa@Ni@*Pm*HAS) microgels containing an NTA amount of 1 mol% show a strong increase in the immobilized enzyme concentration and the amount of formed UDP. Next to the increased enzyme concentration, a reduction of adverse NTA-His interactions could contribute to the higher amount of formed UDP. Table S3 (Supporting Information) hereby shows the ratio of NTA coordination sites to His groups in the His_6-Tag of the enzyme.

When comparing these results to p(VCL/NTAaa@Ni@*Pm*HAS) with χ_{NTA} = 2.2 mol%, the increased enzyme concentration in the sample is also observed. Even so, only a small increase of the UDP formation could be achieved, followed by rather similar UDP concentrations for enzyme concentrations of 2.85 mg mL^{-1} and above. In general, the UDP formation ability of this microgel is much lower than for the microgel containing 1 mol% NTA. This effect could be caused by the higher amount of Ni^{2+} in the system. As previously mentioned, the presence of Ni^{2+} in the solution can have strong deactivating effects on *Pm*HAS,[51] which could also be the case for its complex version. The Ni^{2+} concentration in microgels containing 1 mol% NTA was determined to be 0.199 µmol mL^{-1}. The 2.2-fold concentration would be 0.438 µmol mL^{-1}, making deactivating effects much more likely. Eisele et al.[51] showed almost complete deactivation of *Pm*HAS for Ni^{2+} concentration as low as 1 mM, so a deactivation at a concentration of 0.4 mM for non-complexed Ni^{2+} is inevitable. The effect of complexed metal ions could be less prominent, as complexed metal ions are not able to diffuse freely within the enzyme structure where they can cause deactivating effects. However, our results indicate that also complexed Ni^{2+} leads to partial deactivation of *Pm*HAS. It is noticeable that the microgel with χ_{NTA} = 2.2 mol% is able to immobilize a slightly lower enzyme amount at 1.5 mg mL^{-1}. This additional effect further reduces the overall performance of this enzyme-microgel hybrid. It may be caused by the different morphology of the microgels which was observed through AFM imaging (Figure 1, Figure S8, Supporting Information). A different distribution of NTA in the microgels could influence the overall *Pm*HAS uptake. Even so, the main effect here is not caused by the lower *Pm*HAS uptake: at similar *Pm*HAS contents, the 1 mol% microgels still perform significantly better, further undermining partial *Pm*HAS deactivation at higher NTA and Ni^{2+} concentrations.

In summary, the previous results render p(VCL/NTAaa@Ni@*Pm*HAS) with χ_{NTA} = 1 mol% the most promising microgel for HA synthesis.

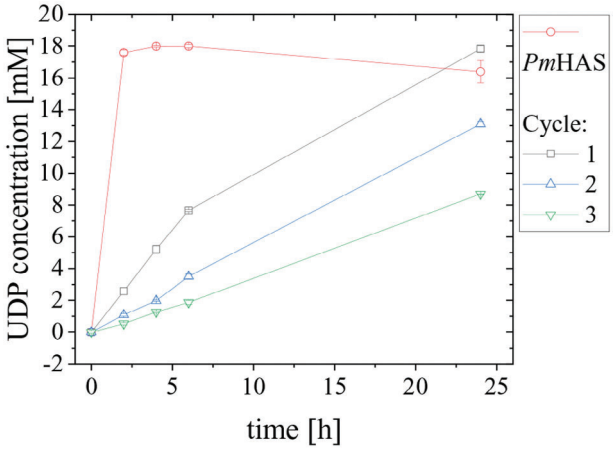

Figure 4. Comparison of p(VCL/NTAaa@Mt@*Pm*HAS) samples during different recycling steps (three cycles) regarding the UDP formation over time as obtained from CE measurements. The microgel samples are compared to pure *Pm*HAS.

2.3.4. Enzyme Recycling

The p(VCL/NTAaa@Ni@*Pm*HAS) microgel (χ_{NTA} = 1 mol%) was then tested regarding its recycling ability, using a concentration of 2.1 mg mL^{-1} purified *Pm*HAS for enzyme immobilization. The enzymatic HA formation was left to proceed for 24 h, followed by a separation of the microgel hybrid from the reaction solution and a repetition of HA formation with fresh substrate solution. The p(VCL/NTAaa@Ni@*Pm*HAS) recycling was repeated twice so that the three resulting time curves can be seen in **Figure 4**.

Obtained p(VCL/NTAaa@Ni@*Pm*HAS) hybrid microgels show a very high UDP concentration after only 24 h. When comparing the UDP formation rate of the hybrid microgel (first cycle) and the purified enzyme, it is visible that the reaction is slower. This phenomenon has also been shown for the previously used microbeads in the work of Gottschalk et al.[6] and might be explained by the hindered substrate diffusion as well as a lower total *Pm*HAS concentration in the microgel samples. Even so, the reached UDP values are almost as high (17.8 mM after 24 h) as the maximum UDP concentration of the purified enzyme (18.0 mM

after 6 h). The amount of formed UDP decreases with each recycling step. We assume that this decrease in enzyme activity is due to partial deactivation or partial loss of the enzyme due to the weak affinity binding interactions. During work-up by centrifugation at high speeds, we observed the formation of a strongly pelleted enzyme-microgel hybrid, so only negligible loss is expected. Moreover, the HA formed in each cycle may hinder substrate and product transfer owing to electrostatic repulsion and steric interactions. Due to the direct repetition of HA formation, achieved by separating HA from the microgel without subsequent washing steps, we can assume that residual HA remains in the reaction solution, influencing the reaction speed. In the first cycle, 17.8 mM UDP was formed (89% of the maximum UDP concentration), in the second cycle 13.1 mM (66%), and in the third cycle 8.7 mM (44%). These values are higher than the ones achieved with magnetic beads where the UDP concentrations were 12.2 mM (61%), 11.1 mM (55%), and 7.8 mM (39%).[6]

We can conclude that the high enzymatic activity and the use of microgels as the enzyme carrier give us an increased number of possible applications. Other than the previously used His Mag Sepharose Ni beads[6] the biocompatibility of p(VCL/NTAaa) microgels has been proven.[30] While the leaching of metal ions can affect biocompatibility,[52] the concentrations in the microgel dispersions used are much below previously shown limits.[53,54] Hence, the application in biological contexts should be feasible. Among others, the microgels could serve as a foundation for designing adaptive hydrogel materials, drawing inspiration from natural mucin's ability to generate polysaccharides. Additionally, scaling up the synthesis of our developed microgels in the future should facilitate the production of a larger quantity of HA which is widely needed in medical[1,2] or cosmetic[3] applications.

2.4. Characterization of the Formed Hyaluronic Acid

In a further step, we wanted to characterize the formed HA regarding its molecular weight and composition using SEC and FT-IR spectroscopy. Therefore, HA was separated from the microgels through centrifugation. The SEC data is shown in **Figure 5** and shows similar molecular weights M_w for all cycles, however slightly decreasing with each cycle (1: 1.74 MDa, 2: 1.61 MDa, 3: 1.55 MDa). The resulting dispersities show relatively low values and a tendency to decrease with each cycle of HA formation (1st cycle: 1.24, 2nd cycle: 1.19, 3rd cycle: 1.12). Jing et al.[55] have previously shown that *Pm*HAS initially forms HA oligosaccharides in a slow initiation step, which are then elongated to form HA polysaccharides. If many HA oligosaccharides are present in the solution, the resulting HA polysaccharides can show a more similar chain length and lower molecular weight.[50,55] We, therefore, believe that with each recycling step, a larger amount of HA oligosaccharides are initially present, resulting in an overall lower molecular weight as well as low dispersities.

The samples were analyzed using SEC and compared to purified *Pm*HAS. Compared to the work of Gottschalk et al.[6] (1st cycle: 1.2 MDa, 2nd cycle: 2.3 MDa, 3rd cycle: 2.8 MDa), the molecular weights M_w are lower but more uniform. The fact that we can fabricate HA of similar molecular weights could be useful for applications where we would need several batches of HA with the same molecular weight. Comparing our M_w to the one of

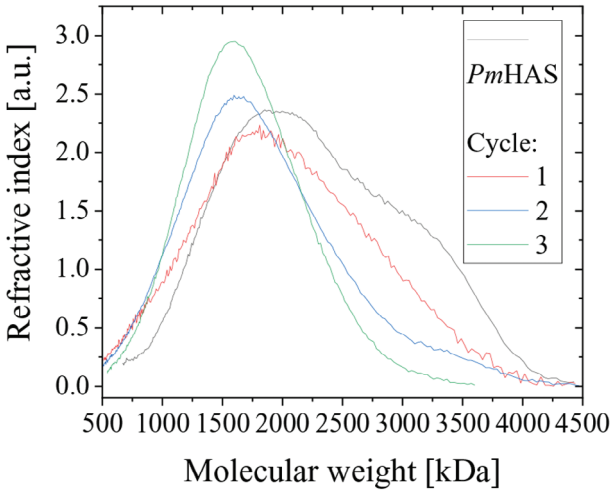

Figure 5. Comparison of p(VCL/NTAaa@Mt@PmHAS) samples after different recycling steps (three cycles) regarding the molecular weight of formed HA (SEC data).

Gottschalk et al.[6] we have to consider the different methods that were used for the determination. This way, the comparability is very limited. Our resulting dispersities of 1.12-1.24 are comparable to the one of the purified enzyme, where a dispersity of 1.15 and a molecular weight of 2.03 MDa were reached. Despite these comparable dispersities, we can see, that the shoulder that is present in the molecular weight distribution of HA formed from purified enzyme is barely visible for the HA formed with our p(VCL/NTAaa@Ni@*Pm*HAS) hybrid microgels. The first cycle still shows indications of a shoulder, while it has completely disappeared for the second and third cycles. It is important to mention that the HA formed by both purified *Pm*HAS and the hybrid microgels in the initial cycle does not present a completely unimodal molecular weight distribution as per SEC. Hence, it is essential to recognize that the calculated M_w and dispersity may vary, given that the calculation relies on an unimodal curve. To conclude, we can see a more uniform molecular weight distribution compared to the purified enzyme even though the dispersities are similar. Regarding the higher molecular weight obtained with the purified enzyme, we have to take into account that the contact with the enzyme was much longer compared to the p(VCL/NTAaa@Ni@*Pm*HAS) samples, where the HA/substrate solution was separated from the microgel hybrid directly after each 24 h cycle. The SEC results are summarized in Table S4 (Supporting Information).

The formed HA was further investigated by FT-IR spectroscopy using a commercial HA sodium salt as a reference. The spectra are shown in Figure S12 (Supporting Information) and show overlapping signals for all major functional groups. There are a few deviations between the recorded spectra which is explained due to the presence of protonated carboxylic groups in our sample, whereas the commercial HA is purely present as its sodium salt. The comparison to previous works [56,57] confirms our peak assignments.

Using FT-IR spectroscopy and SEC, we were able to demonstrate the successful enzymatic synthesis of HA. Compared to previous works, we have achieved an exceptionally high UDP

yield after three cycles of *Pm*HAS, facilitating the production of high molecular weight HA with high yields.

Furthermore, the constructed p(VCL/NTAaa) microgls can be used for the immobilization of a variety of other enzymes containing a His_6-Tag.

3. Conclusion and Future Perspectives

In this work, we synthesized poly(*N*-Vinylcaprolactam-2,2′-((5-acrylamido-1-carboxypentyl)azanediyl)diacetic acid) (p(VCL/NTAaa)) core–shell microgels containing different amounts of nitrilotriacetic acid (NTA), localized in the microgel shell. Characterization via FT-IR spectroscopy, zeta potential measurements, and dynamic light scattering confirmed the successful incorporation of the co-monomer in low polydispersity microgels. Furthermore, AFM was performed, revealing the core–shell morphology of the microgels, which became visible at higher NTA contents due to the increased thickness of the NTA-rich microgel shell. This core–shell structure is particularly advantageous for the immobilization enzymes. It enhances the accessibility of the NTA units for enzyme attachment and improves the diffusion of substrates and products to and from enzymes. Furthermore, the enzymatic products are easily separated from the microgels through centrifugation, facilitated by the denser core of the microgel. In addition to facilitating simple separation from reaction products, the microgel core also ensures the stability of the microgels.

NTA groups in the microgel structure were used for the complexation of Ni^{2+}, Co^{2+}, Mn^{2+}, Mg^{2+}, and $Fe^{2+/3+}$ which was confirmed by ICP-OES and zeta potential measurements. The enzyme Hyaluronan Synthase from *Pasteurella multocida* (*Pm*HAS) was then bound to the microgels via an incorporated polyhistidine tag (His_6-Tag), enabling the formation of an enzyme-NTA complex. Through observation of the UDP formation during HA synthesis, capillary electrophoresis analysis indicated that p(VCL/NTAaa@Ni) microgels were the most suited for *Pm*HAS immobilization and HA production. Further experiments with a library of p(VCL/NTAaa@Ni) microgels revealed an initial increase in *Pm*HAS activity followed by a decrease with increasing NTA content, due to interactions of Ni^{2+} with His groups in the enzyme.

Previously, only a few studies have been published on HA synthesis and, more specifically, high molecular weight HA synthesis using immobilized *Pm*HAS. Among these studies, the herein presented p(VCL/NTAaa@Ni) microgels stand out with exceptionally high yields of UDP and HA. Our optimization process led to the formation of a hybrid microgel with maximum productivity. This represents a noteworthy achievement in high molecular weight HA production, which was further extended by demonstrating reusability for three cycles over 24 h. Additionally, we demonstrated predominantly consistent molecular weights from cycle to cycle, a crucial feature for future industrial-scale applications, given the significant dependence of HA's biological functions on its molecular weight. Moving forward, efforts should prioritize scaling up the synthesis to produce larger quantities of HA.

Looking toward future perspectives, a wider variety of applications of the presented p(VCL/NTAaa) microgels can be enabled. In addition to their ideal properties for PmHAS immobilization and HA production, these microgels have the potential to immobilize various other enzymes containing a His-Tag, expanding the applications to the enzymatic production of a variety of other products. Moreover, beyond enzyme immobilization, the microgels could be engineered with dual functionality. For instance, enzymes could be immobilized in the microgel shell while specific molecules are incorporated in the core, allowing for simultaneous drug delivery, among others. Finally, microgels containing immobilized *Pm*HAS can be valuable for designing adaptive, self-regenerating hydrogel materials. The microgels have the capability to continuously produce HA by supplying enzyme substrates, a process similar to natural polysaccharide production in mucin. Here, the continuous formation of a protective, lubricant polysaccharide layer provides materials with self-regenerating properties. In summary, the versatility of these microgels warrants extensive future research and exploration across diverse applications.

4. Experimental Section

Materials: Reaction solvents were of analytical grade and were used as received from Omnisolv. Ultra-pure water (Merck, HPLC grade) was employed for aqueous reactions. *N*-Vinylcaprolactam (VCL, Sigma-Aldrich, 98%) was distilled and recrystallized from hexane before use. The crosslinker *N*,*N*′-methylenebis(acrylamide) (BIS, Sigma-Aldrich, 99%), the initiator 2,2′-azobis(2-methylpropionamidine)dihydro-chloride (AMPA, Sigma-Aldrich, 97%) and the stabilizer cetyltrimethylammonium bromide (CTAB, Carl Roth, 99%) were used as received. For the preparation of buffers, ammonium acetate (Carl Roth, 97%), ethylenediaminetetraacetic acid (EDTA, Sigma-Aldrich, 99%), *N*-(2-hydroxyethyl)piperazine-N′-(2-ethanesulfonic acid) (HEPES, Sigma-Aldrich, 99%) and sodium hydroxide (NaOH, Merck, 99.5%) were used. Enzyme production involved the use of isopropyl *β*-D-1-thiogalactopyranoside (IPTG, AppliChem GmbH, 99%), yeast extract (Serva), tryptone (Carl Roth) and ampicillin sodium salt (Carl Roth, 97%). Furthermore, agar-agar (Carl Roth), potassium hydrogen phosphate (Carl Roth, 98%), potassium dihydrogen phosphate (Carl Roth, 98%), NaCl (Carl Roth, 99,5%), and imidazole (PanReac AppliChem) were ordered. The following metal salts were used for incorporation into microgels or as co-factors for the enzyme *Pm*HAS: $CoCl_2 \cdot 6\ H_2O$ (Sigma Aldrich, 98%), $FeSO4 \cdot 7\ H_2O$ (Sigma Aldrich, 99%), $FeCl_2 \cdot 4\ H_2O$ (Sigma Aldrich, 99%), KCl (Sigma Aldrich, 85%), $MnCl_2 \cdot 4\ H_2O$ (Sigma Aldrich, 98%), $MgSO_4$ (Sigma Aldrich, 99.5%), $NiSO_4 \cdot 6\ H_2O$ (Sigma Aldrich, 98%). Furthermore, the enzyme substrates, uridine diphosphate glucuronic acid (UDP-GlcA, Carbosynth or Sigma Aldrich, 98%) and uridine 5′-diphospho-*N*-acetylglucosamine sodium salt (UDP-GlcNAc, Carbosynth or Sigma Aldrich, 98%) were used, as well as *para*-aminobenzoic acid (PABA Sigma Aldrich, 99%), *para*-aminophtalic acid (PAPA, Sigma Aldrich, 97%) and sodium dodecyl sulfate (SDS ≥99.8 Roth). DOWEX 50WX8, hydrogen form, 100–200 mesh (Sigma Aldrich) Roti-Quant (Carl Roth), *N*,*N*'-bis(carboxymethyl)-L-lysine, acryloyl chloride (Sigma-Aldrich, 97%) and sulphuric acid (H_2SO_4, Sigma Aldrich, 95%) were further used during monomer synthesis. For size exclusion chromatography, water (HiPerSolv CHROMANORM HPLC grade, VWR), Na_2HPO_4 (Carl Roth, 99%), 0.069 NaCl (Bernd Kraft, 99%), dextran standards (Polymer Standards Service) and ethylene glycol (Fluka analytical, 99.5%) were purchased. Further measurements required the use of HNO_3. (Carl Roth, 95%)

Enzyme Production: His_6-tagged *Pm*HAS1-703 was produced according to previous works of Gottschalk et al.[50,51] Therefore, plasmids were transformed into E. coli BL21 (DE3) via heat shock. Positive clones were selected on agar plates with lysogeny broth (LB) and ampicillin (100 µg mL−1). 20 mL LB medium with ampicillin was inoculated with positive clones. The preculture was cultivated in a 100 mL baffled flask (18 h, 37 °C, 120 rpm). From the preculture medium, 20 mL was used to inocu-

late 1 L terrific broth medium in a 5 L baffled flask (37 °C, 80 rpm). Cells were grown to an optical density of 0.6-0.8 at 600 nm. The expression was initiated with 0.1 mM IPTG and the temperature was lowered to 25 °C. The cultivation was centrifuged (7000 rpm, 30 min, 4 °C) after 20 h. After pouring off the supernatant, the remaining cells were stored at −20 °C. 4 g of frozen cells were dispersed in 10 mL of binding buffer (20 mM sodium phosphate, 500 mM sodium chloride, 30 mM imidazole, pH 7.4). The cells were disrupted using ultrasound (6:30 min, 15 s pulse, 60 s pause, 52% amplitude) and then separated via centrifugation (15 000 rpm, 30 min, 4 °C). The crude extract containing *Pm*HAS was filtered using a 0.8 µm filter. Immobilized metal ion affinity chromatography (IMAC) on 5 mL His-Trap HP columns (GE Healthcare) was used for the purification of the recombinant enzymes. The purification process was executed on the ÄKTApurifier 100 (GE Healthcare) under the control of the Unicorn program. Side products were removed by washing with 20 mM Na_2HPO_4, 500 mM NaCl, and 30 mM imidazole brought to pH 7.4. *Pm*HAS was subsequently eluted using an elution buffer composed of 20 mM Na_2HPO_4, 500 mM NaCl, and 500 mM imidazole, with a pH of 7.4. For buffer exchange, dialysis was performed, employing 100 mM HEPES at pH 8, storing the resulting product at 4 °C. The protein concentration was determined through a Bradford protein assay.

Synthesis of 2,2′-((5-acrylamido-1-carboxypentyl)azanediyl)diacetic Acid: 2,2′-((5-acrylamido-1-carboxypentyl)azanediyl)diacetic acid (NTAaa) was synthesized according to Mizrahi et al.[23] and adapted in the previous publication.[30] *N,N′*-bis(carboxymethyl)-L-lysine (1.6 g, 6.10 mmol) was dissolved in 0.4 M NaOH (50 mL) and a solution of acryloyl chloride (530 µL, 6.52 mmol) in toluene (25 mL) was added dropwise while cooling with ice. After stirring overnight, toluene was evaporated at reduced pressure. Residual sodium ions were removed using pre-washed DOWEX 50WX8 by mixing the ion exchanger with the reaction solution for several hours. After filtering off DOWEX 50WX8, it was washed with water until reaching a neutral pH. The product was dried via lyophilization to yield a white powder. Characterization was done by NMR spectroscopy (Figure S1, Supporting Information).

^{1}H-NMR (400 MHz, DMSO-d_6, $\delta = 2.50$): δ = 8.16 (t, 1H, NH), 6.21 (dd, 1H, CH), 6.03 (dd, 1H, CH), 5.53 (dd, 1H, CH), 3.46 (q, 4H, CH2), 3.32 (t, 1H, CH), 3.07 (q, 2H, CH2), 1.56 (m, 2H, CH2), 1.40 (m, 2H, CH2), 1.28 (m, 2H, CH2) ppm.

Synthesis of Dimethyl 2,2′-((6-acrylamido-1-methoxy-1-oxohexan-2-yl)azanediyl) Diacetate: As described in the previous publication,[30] the carboxylic groups of NTAaa were methylated to facilitate its subsequent polymerization. NTAaa (1.299 g, 4.1 mmol) was dissolved in MeOH (26 mL) mixed with concentrated sulphuric acid (221 µL). After refluxing the solution for 3 h at 65 °C, the majority of the solvent was removed to reach a volume of ≈5 mL. After the addition of DCM, the product was extracted using saturated solutions of $NaHCO_3$ (2 × 50 mL) and NaCl (1 × 50 mL) in water. Residual water was removed from the solution by drying over anhydrous Na_2SO_4. After removing the remaining solvent, the product was dried in an ultra-high vacuum. The resultant product appeared as a yellow, highly viscous liquid (889.8 mg, 2.5 mmol, 60%), and its characterization was conducted through NMR spectroscopy (Figure S2, Supporting Information)).

For further use, the formed monomer dimethyl 2,2′-((6-acrylamido-1-methoxy-1-oxohexan-2-yl)azanediyl)diacetate (NTAMaa) was stored in dimethyl sulfoxide (DMSO) at a concentration of 17.9 mg mL^{-1}.

^{1}H-NMR (400 MHz, DMSO-d_6, $\delta = 2.50$): δ = 8.04 (t, 1H, NH), 6.19 (dd, 1H, CH), 6.04 (dd, 1H, CH2), 5.54 (dd, 1H, CH2), 3.58 (m, 13H, CH2, CH3), 3.39 (t, 1H, CH), 3.08 (m, 2H, CH2), 1.57 (m, 2H, CH2), 1.40 (m, 2H, CH2), 1.22 (m, 2H, CH2) ppm.

Microgel Synthesis: To synthesize poly(*N*-vinylcaprolactam-2,2′-((5-acrylamido-1-carboxypentyl)azanediyl)diacetic acid) (p(VCL/NTAaa)) microgels, a semi-batch precipitation polymerization was carried out.[30] VCL (275.6 mg, 1.98 mmol, 99 mol%), BIS (8.0 mg, 0.05 mmol, 2.6 mol%), and CTAB (1.2 mg, 0.003 mmol, 0.1 mol%) were dissolved in H_2O (13.5 mL) and heated to 70 °C while degassing the solution. For this, the solution was purged using nitrogen. The initiator AMPA (6.6 mg, 0.02 mmol, 1.2 mol%) was then added in 0.5 mL H_2O via a syringe. After 25 to 45 s, a solution of NTAMaa (7.2 mg, 0.02 mmol, 1 mol%) in DMSO (6 mL) was continuously added within 8 min utilizing a syringe pump, followed by 5 h of stirring at 70 °C. After cooling down to room temperature, NaOH (1.5 mL, 0.1 M) was added to the resulting p(VCL/NTAMaa) microgel dispersion, which was then stirred for 24 h. The purification was enabled by dialysis against water for five days. For this, the microgel solution was placed into dialysis membranes(regenerated cellulose membrane, MWCO = 12 – 14 kDa), and the water was exchanged three to five times a day against fresh demineralized water. The microgels were lyophilized and obtained as a white powder. To synthesize microgels with varying comonomer content, the ratio of VCL to NTAMaa was adjusted. The NTAaa content was determined via FT-IR spectroscopy. For this, the peak ratio (PR) of maximum absorbance between 1750-1700 cm^{-1} divided by the maximum absorbance between 1650-1580 cm^{-1} was used. The equation for the determination of the NTAaa amount χ_{NTA} was determined in previous works:[30] $PR = -0.07118 + 0.34956 \cdot \log_{10}(\chi_{NTA})$.

PVCL microgels were synthesized through a batch polymerization process. A solution of VCL (2.0879 g, 15 mmol, 100 mol%) and BIS (60.1 mg, 0.39 mmol, 2.6 mol%) in H_2O (149 mL) was degassed and heated to 70 °C. The initiation of the reaction occurred through the addition of AMPA (48.8 mg, 0.18 mmol, 1.2 mol%) in H_2O (1 mL). After 3 h, the flask was left to cool down to room temperature while stirring continuously. The microgels were purified via dialysis (regenerated cellulose membrane, MWCO = 12 – 14 kDa, 5 days) against water and lyophilized.

Incorporation of Metal(II) Ions into Microgels: To the p(VCL/NTAaa) samples (5 mg), a metal (Mt) salt solution was added (0.75 M, 1 mL) for which the following salts were used: $CoCl_2 \cdot 6\,H_2O$, $FeCl_2 \cdot 4\,H_2O$, $MnCl_2 \cdot 4\,H_2O$, $MgSO_4$, $NiSO_4 \cdot 6\,H_2O$. The samples were placed in a head-over-head shaker for at least 12 h. Purification was carried out by dialysis against water using a regenerated cellulose membrane (MWCO = 12 – 14 kDa) for 5 days. After lyophilization, the p(VCL/NTAaa@Mt) microgels were yielded as slightly colored to white powders.

Immobilization of PmHAS into Microgels: For immobilization of His_6-tagged *Pm*HAS into p(VCL/NTAaa@Mt) microgels, the samples were dissolved in HEPES (100 mM, pH 8) and mixed with enzyme stock solution to achieve final concentrations of 3.0 mg mL^{-1} microgel and 1.5 mg mL^{-1} purified *Pm*HAS. After incubation at 4 °C for at least 2 full days, the residual enzyme was removed by centrifugation (3 × 10 000 rpm, 4 °C, 30 min). After each centrifugation step, the p(VCL/NTAaa@Mt@*Pm*HAS) microgels were redispersed in HEPES (100 mM, pH 8), maintaining the previous microgel concentration.

Production of Hyaluronic Acid and Enzyme Activity Assay: For the production of HA by the enzymatic activity of *Pm*HAS, a substrate solution was prepared. *Pm*HAS catalyzes the formation of HA from uridine diphosphate glucuronic acid (UDP-GlcA) and UDP *N*-acetylglucosamine (UDP-GlcNAc) precursors[7,55] and could elongate supplied HA oligosaccharides.[55] The emerging glycosaminoglycan HA was thereby assembled from alternating GlcA and GlcNAc groups linked via alternating β-(1→3) and β-(1→4) glycosidic bonds.[9]

Therefore, the nucleotide sugars UDP-GlcA trisodium salt (58.1 mg, 0.09 mmol) and UDP-GlcNAc disodium salt (58.6 mg, 0.09 mmol) and the enzyme cofactors $MgCl_2 \cdot 6\,H_2O$ (27.4 mg, 0.135 mmol), KCl (6.8 mg, 0.09 mmol) and $MnCl_2 \cdot 4H_2O$ (2.7 mg, 0.0135 mmol) were dissolved in HEPES (100 mM, pH 8, 1.8 mL). Furthermore, an aqueous (50 mL) stop solution, inhibiting further production of HA was prepared from SDS (201.9 mg, 14 mM), PABA (137 mg, 2 mM), and PAPA (18.1 mg, 2 mM). 200 µL substrate solution was mixed with 800 µL test solution, which was the previously obtained p(VCL/NTAaa@Mt@*Pm*HAS) solution or a control sample containing enzyme solution without microgels. In this mixture, final concentrations of 15 mM Mg^{2+}, 10 mM K^+, and 1.5 mM Mn^{2+}, were employed, as they had been previously reported to provide optimal conditions for achieving high conversion rates.[50,51] The concentrations of UDP-GlcA and UDP-GlcNAc were both set at 10 mM consistent with previous studies.[6,50] For investigation of HA formation at different time points, samples were taken after 0, 2, 4, 6, 25, and 54 h. For this 45 µL of the sample containing the test solution and substrate solution were mixed with 45 µL of stop solution. For enzyme recycling tests, the mixtures were centrifuged (3 × 10 000 rpm, 4 °C, 30 min), filled up to 800 µL using 100 mM HEPES at pH 8, followed by the addition of substrate so-

lution (200 µL). The samples were then stored at −20 °C until they were investigated by Multiplexed Capillary Electrophoresis (MP-CE).

Analytical Methods—Nuclear Magnetic Resonance Spectroscopy: Nuclear magnetic resonance (NMR) measurements were performed at room temperature, using a Bruker DPX-400 FT-NMR spectrometer at 400 MHz. Freeze-dried microgel samples were dissolved in D_2O or DMSO-d6 for NMR analysis.

Analytical Methods—Fourier-Transform Infrared Spectroscopy: Fourier-transform infrared (FT-IR) spectroscopy was conducted in the range of 4000 to 400 cm^{-1} with a resolution of 4 cm^{-1} and 4 scans per measurement. For this, samples were placed on a diamond crystal plate of an FTIR-Spectrum 3 by PerkinElmer using a GladiATR Single reflection by PIKE Technologies. Before sample measurement, a background measurement was conducted. The software Spectrum v10.7.2. was used to record measurements and the spectra were baseline-corrected and normalized.

The NTA contents in different p(VCL/NTAaa) microgels were determined according to the following equation: [30]

$$\chi_{NTA} = 10^{(PR+0.07118)\cdot 0.034956^{-1}} \quad (1)$$

Analytical Methods—Dynamic Light Scattering: Dynamic light scattering (DLS) measurements were performed using a Malvern Instruments Zetasizer Ultra Pro. For this purpose, samples were diluted in ultrapure water to a concentration of 0.5 mg mL^{-1}. They were then placed in square 12 mm polystyrene DTS0012 cuvettes. For each sample, three measurements were performed, each with 5 runs at 25 °C, using a scattering angle $\theta = 90°$. ZS Xplorer software was used to analyze the results.

Analytical Methods—Electrophoretic Light Scattering: The Zetasizer Ultra Pro from Malvern Instruments was also used for electrophoretic light scattering (ELS) measurements for zeta potential analysis. Samples were placed into disposable folded capillary cells (DTS1070) at a concentration of 0.5 mg mL^{-1} in ultrapure water. For each sample, three measurements were performed at 25 °C with up to 100 runs each, and the data were analyzed using ZS Xplorer software. Measurements were performed at a scattering angle of $\theta = 12.8°$ and an applied voltage of 150 V.

Analytical Methods—Multiplexed Capillary Electrophoresis: Multiplexed capillary electrophoresis (MP-CE) measurements were conducted using a multiplexed cePRO 9600TM system which was operated by the pKa-analyzer software (Advanced Analytical Technologies. Ames. IA. USA). The enzymatic reaction of *Pm*HAS was analyzed by the separation of the nucleotide sugars (UDP-GlcA and UDP-GlcNAc) and nucleotides (UDP and uridine monophosphate (UMP)). This method had been previously reported by Gottschalk et al.[6] Therefore, a 96-capillary array was used, enabling the measurement of multiple samples simultaneously. Each capillary possesses an inner diameter of 50 µm and an effective and total length of 55 and 80 cm respectively. Before separation, the system was washed with 0.1 M NaOH, followed by water. Samples were injected by vacuum (−0.7 psi, 10 s), followed by the separation of the substances by applying a voltage of 10 kV. 70 mM ammonium acetate containing 1 mM EDTA at pH 9.2 was used as the electrophoresis buffer and PABA and PAPA acted as internal standards with a concentration of 1 mM each. After the analytes were detected by UV light (254 nm), the resulting data was evaluated by the pKa-analyzer software. The amount of the analytes was calculated using the peak areas.

Analytical Methods—Inductively Coupled Plasma Optical Emission Spectroscopy: Inductively coupled plasma optical emission spectroscopy (ICP-OES) measurements were conducted to determine the metal content in microgels. Therefore, the samples were solubilized in 3 mL HNO_3 in the microwave. The measurement was then conducted on a PlasmaQuant PQ9000 Elite and analyzed with the program Jena.

Analytical Methods—Bradford Protein Assay: Roti-Quant (10 mL) was diluted with purified water (27.5 mL) to obtain the Bradford reagent. The test solution of 6 µL was diluted in water (HPLC grade) to a suitable concentration. Of each sample, 25 µL was placed onto a well plate and 100 µL Bradford reagent was added to each well. After an incubation time of 11.5 min, the absorbance was measured at a wavelength of 595 nm using a Multi-Mode Microplate Reader Synergy 2 (BioTek. Vermont. USA). Samples were measured threefold. The calibration was performed with a bovine serum albumin standard following the same experimental procedure.

Analytical Methods—Atomic Force Microscopy: Atomic force microscopy was recorded in tapping mode using a NanoScope V from Veeco Instruments. An NCH-50 POINTPROBE silicone SPM sensor from Nanoworld with a resonant frequency of 320 kHz and a force constant of 42 Nm^{-1} served as the cantilever. For microgel imaging, the microgels were spin-coated on plasma-activated Si-wafers. The analysis of the AFM images was performed using the Gwyddion software.

Analytical Methods—Size Exclusion Chromatography: A neutral to anionic size exclusion chromatography (SEC) setup was used for the determination of molecular weights (M_w and M_n) and molecular weight distributions (M_w/M_n). Water, containing 0.005 M Na_2HPO_4 and 0.069 NaCl at pH 3.9, served as the eluent. The samples contained ethylene glycol (0.7 µL mL^{-1}) as an internal standard. The device was operated with an HPLC pump (1200, Agilent), and was equipped with a refractive index (RI) detector (1200, Agilent) and a UV detector (VWD, 1200, Agilent). For separation, one pre-column (8 × 50 mm) and three Suprema-Lux gel columns (8 × 300 mm, Polymer Standards Service) were used at a flow rate of 1.0 mL min^{-1} and 40 °C. The nominal pore widths were 30, 1000, and 1000 Å with gel particles of 5 µm diameter. For calibration, narrowly distributed Dextran standards (Polymer Standards Service) were used. The evaluation of the results was performed using PSS WinGPC UniChrom software (Version 8.3.2).

Supporting Information

Supporting Information is available from the Wiley Online Library or from the author.

Acknowledgements

The financial support of the project MiRAGE (031B1116A and 031B1116B) from the BMBF (Federal Ministry of Education and Research, Germany) within the project cluster "Future technologies for the industrial bioeconomy: focus on biohybrid technology" was greatly acknowledged. The authors thank Pham Truc and Kai P. Hussnaetter for repetitive enzyme production and Bradford measurements. Further, the authors extend gratitude to Renate Jansen for ICP-OES measurements, and Dr. Michael Pohl and Rainer Haas for the acquisition of SEC data. The contributions of Johannes Gottschalk regarding preliminary tests were gratefully acknowledged. Furthermore, the assistance of Hannes Frohnmeyer with MP-CE measurements was much appreciated. Parts of the analytical investigations were performed at the Center for Chemical Polymer Technology CPT, which was supported by the European Commission and the federal state of North Rhine-Westphalia (No. 300088302).

Open access funding enabled and organized by Projekt DEAL.

Conflict of Interest

The authors declare no conflict of interest.

Data Availability Statement

The data that support the findings of this study are available from the corresponding author upon reasonable request.

Keywords

biomaterials, enzyme immobilization, metal affinity binding, microgels, polysaccharides

Received: February 20, 2024
Revised: May 23, 2024
Published online:

[1] Hansen, I. M., Ebbesen, M. F., Kaspersen, L., Thomsen, T., Bienk, K., Cai, Y., Malle, B. M., Howard, K. A., *Mol. Pharmaceutics* **2017**, *14*, 2359.
[2] N. M. Salwowska, K. A. Bebenek, D. A. Żądło, D. L. Wcisło-Dziadecka, *J Cosmet Dermatol* **2016**, *15*, 520.
[3] A. M. Juncan, D. G. Moisă, A. Santini, C. Morgovan, L. L. Rus, A. L. Vonica-Țincu, F. Loghin, *Molecules* **2021**, *26*, 4429.
[4] M. Qiao, J. Zhang, J. Li, L. Xing, X. Zhou, Y. Xie, X. Zhang, *Process Biochem* **2023**, *133*, 261.
[5] Y. Qiu, Y. Ma, Y. Huang, S. Li, H. Xu, E. Su, *Carbohydr. Polym.* **2021**, *269*, 118320.
[6] J. Gottschalk, M. Aßmann, J. Kuballa, L. Elling, *ChemSusChem* **2022**, *15*, 202101071.
[7] J. Gottschalk, L. Elling, *Curr. Opin. Chem. Biol.* **2021**, *61*, 71.
[8] J. H. Sze, J. C. Brownlie, C. A. Love, *Biotech* **2016**, *6*, 67.
[9] P. L. DeAngelis, *Cell. Mol. Life Sci.* **1999**, *56*, 670.
[10] P. L. DeAngelis, J. Zimmer, *Glycobiology* **2023**, *33*, 1117.
[11] M. Nöth, E. Gau, F. Jung, M. D. Davari, I. El-Awaad, A. Pich, U. Schwaneberg, *Green Chem.* **2020**, *22*, 8183.
[12] A. A. Homaei, R. Sariri, F. Vianello, R. Stevanato, *J Chem Biol* **2013**, *6*, 185.
[13] P. Torres-Salas, A. Del Monte-Martinez, B. Cutiño-Avila, B. Rodriguez-Colinas, M. Alcalde, A. O. Ballesteros, F. J. Plou, *Adv. Mater.* **2011**, *23*, 5275.
[14] R. A. Sheldon, *Adv. Synth. Catal.* **2007**, *349*, 1289.
[15] M. N. Gupta, M. Kaloti, M. Kapoor, K. Solanki, *Art. Cells, Blood Subs., and Immob.* **2011**, *39*, 98.
[16] R. A. Sheldon, A. Basso, D. Brady, *Chem. Soc. Rev.* **2021**, *50*, 5850.
[17] L. Cao, *Curr. Opin. Chem. Biol.* **2005**, *9*, 217.
[18] M. Karg, A. Pich, T. Hellweg, T. Hoare, L. A. Lyon, J. J. Crassous, D. Suzuki, R. A. Gumerov, S. Schneider, I. I. Potemkin, W. Richtering, *Langmuir* **2019**, *35*, 6231.
[19] F. A. Plamper, W. Richtering, *Acc. Chem. Res.* **2017**, *50*, 131.
[20] J. Oberdisse, T. Hellweg, *Colloid Polym. Sci.* **2020**, *298*, 921.
[21] J. M. Guisan, Ed. *Methods in Biotechnology*, Humana Press, Totowa, NJ **2006**, *22*.
[22] J. M. Guisan, Ed. *Methods in Biotechnology*, **2006**, Humana Press, USA **2006**, *22*.
[23] B. Mizrahi, S. Irusta, M. McKenna, C. Stefanescu, L. Yedidsion, M. Myint, R. Langer, D. S. Kohane, *Adv. Mater.* **2011**, *23*, H258.
[24] J. Porath, B. Olin, *Biochem* **1983**, 1621.
[25] V. Gaberc-Porekar, V. Menart, *J. Biochem. Biophys. Methods* **2001**, *49*, 335.
[26] H. Block, B. Maertens, A. Spriestersbach, N. Brinker, J. Kubicek, R. Fabis, J. Labahn, F. Schäfer, *Methods Enzymol* **2009**, *463*, 439.
[27] T. Heida, T. Köhler, A. Kaufmann, M. J. Männel, J. Thiele, *Chem Syst. Chem.* **2020**, *2*, e1900058.
[28] T. Köhler, T. Heida, S. Hoefgen, N. Weigel, V. Valiante, J. Thiele, *RSC Adv.* **2020**, *10*, 40588.
[29] H. Xu, B. Wei, X. Liu, Y. Huang, W. Zhou, H. Liang, *Biochem. Eng. J.* **2022**, *180*, 108362.
[30] I. K. Sommerfeld, H. Malyaran, S. Neuss, D. E. Demco, A. Pich, *Biomacromolecules* **2024**, *25*, 903.
[31] P. L. DeAngelis, L. C. Oatman, D. F. Gay, *J. Biol. Chem.* **2003**, *278*, 35199.
[32] T. Mori, A. Hirose, T. Hagiwara, M. Ohtsuka, Y. Kakuta, K. Kimata, Y. Okahata, *J. Am. Chem. Soc.* **2012**, *134*, 20254.
[33] L. C. Kröger, W. A. Kopp, K. Leonhard, *J. Phys. Chem. B* **2017**, *121*, 2887.
[34] F. Grabowski, V. S. Petrovskii, F. Fink, D. E. Demco, S. Herres-Pawlis, I. I. Potemkin, A. Pich, *Adv. Sci.* **2022**, *9*, e2204853.
[35] H. M. Irving, M. G. Miles, L. D. Pettit, *Anal. Chim. Acta* **1967**, *38*, 475.
[36] A. K. Das, *Transition Met. Chem.* **1990**, *15*, 75.
[37] Y. Tomita, K. Ueno, *Bull. Chem. Soc. Jpn.* **1963**, *36*, 1069.
[38] R. L. Anderson, W. E. Bishop, R. L. Campbell, *Crit. Rev. Toxicol.* **1985**, *15*, 1.
[39] A. E. Martell, R. M. Smith, *Critical Stability Constants: Inorganic Complexes*, Springer, New York, NY **1976**.
[40] A. Mourran, Y. Wu, R. A. Gumerov, A. A. Rudov, I. I. Potemkin, *Langmuir* **2016**, *32*, 723.
[41] L. Hoppe Alvarez, A. A. Rudov, R. A. Gumerov, P. Lenssen, U. Simon, I. I. Potemkin, D. Wöll, *Phys. Chem. Chem. Phys.* **2021**, *23*, 4927.
[42] M. A. Salam, K. Aoki, *Inorg. Chim. Acta* **2000**, *311*, 15.
[43] N. H. Dung, B. Viossat, A. Busnot, J. M. González Pérez, S. González García, *Inorg. Chem.* **1988**, *27*, 1227.
[44] E. Souaya, W. Hanna, E. Ismail, N. Milad, *Molecules* **2000**, *5*, 1121.
[45] M. S. Zetter, M. W. Grant, E. J. Wood, H. W. Dodgen, J. P. Hunt, *Inorg. Chem.* **1972**, *11*, 2701.
[46] R. J. Motekaitis, A. E. Martell, *J. Coord. Chem.* **1994**, *31*, 67.
[47] M. A. Walters, V. Vapnyar, A. Bolour, C. Incarvito, A. L. Rheingold, *Polyhedron* **2003**, *22*, 941.
[48] K. Sawada, W. Duan, M. Ono, K. Satoh, *J Chem Soc 2000, Dalton Trans.* 919.
[49] G. Chaga, D. E. Bochkariov, G. G. Jokhadze, J. Hopp, P. Nelson, *J. Chromatogr. A* **1999**, *864*, 247.
[50] J. Gottschalk, H. Zaun, A. Eisele, J. Kuballa, L. Elling, *Int. J. Mol. Sci.* **2019**, *20*, 5664.
[51] A. Eisele, H. Zaun, J. Kuballa, L. Elling, *ChemCatChem* **2018**, *10*, 2969.
[52] L. Büdinger, M. Hertl, *Allergy* **2000**, *55*, 108.
[53] M. Horie, K. Nishio, K. Fujita, H. Kato, A. Nakamura, S. Kinugasa, S. Endoh, A. Miyauchi, K. Yamamoto, H. Murayama, E. Niki, H. Iwahashi, Y. Yoshida, J. Nakanishi, *Chem. Res. Toxicol.* **2009**, *22*, 1415.
[54] W. Jia, M. W. Beatty, R. A. Reinhardt, T. M. Petro, D. M. Cohen, C. R. Maze, E. A. Strom, M. Hoffman, *J Biomed Mater Res* **1999**, *48*, 488.
[55] W. Jing, P. L. DeAngelis, *J. Biol. Chem.* **2004**, *279*, 42345.
[56] N. C. Pan, H. C. B. Pereira, M. d. L. C. Da Silva, F. D. A. Vasconcelos, M. A. P. C Celligoi, *Appl. Biochem. Biotechnol.* **2017**, *182*, 276.
[57] R. Gilli, M. Kacuráková, M. Mathlouthi, L. Navarini, S. Paoletti, *Carbohydr. Res.* **1994**, *263*, 315.